A Machine Learned Traffic Flow Coordination Framework for Flow-Centric Airspace

Chunyao Ma, Sameer Alam, Qing Cai, Daniel Delahaye

A Machine Learned Traffic Flow Coordination Framework for Flow-Centric Airspace

Chunyao Ma, Sameer Alam, Qing Cai
Air Traffic Management Research Institute
Nanyang Technological University
Singapore
{chunyao.ma|sameeralam|qcai}@ntu.edu.sg

Daniel Delahaye
OPTIM Lab
Ecole Nationale de l'Aviation Civile
Toulouse, France
daniel.delahaye@enac.fr

***Abstract*—Air traffic flow coordination at major flow intersections is a key enabler for flow-centric airspace concepts. This paper develops a flow-centric air traffic flow coordination framework to improve air traffic flow efficiency through flow identification, prediction, and re-routing at the Nominal Flow Intersections (NFIs). To identify the NFIs, a graph-based flow pattern consistency approach is proposed to model and analyze daily air traffic flow patterns. To predict future traffic demands at the identified NFIs, a transformer encoder-based neural network is adopted to learn the relations among the flow of flights at the NFIs. The acceptable flow limits at the NFIs are then determined by phase transitions of the flow efficiency versus the traffic demand. Finally, to avoid the predicted demand exceeding the identified flow limit and improve the flow efficiency, a reinforcement learning-based flow re-routing agent is trained to dynamically assign alternative routes to air traffic flows based on the evolving flow states. The agent's performance is quantified by the flight time reduction in the flows without exceeding the flow limits. The re-routing model is trained and tested on a busy NFI that handles cross-border flows between Bordeaux and Madrid/Barcelona control centers, using ADS-B data for Dec 2019 in European airspace. Results show that, compared with the originally planned flows, the travel time of each flight is reduced by 322.168 seconds on average on a 2-hour basis.**

***Index Terms*—flow coordination, flow-centric, traffic prediction, transformer neural networks, reinforcement learning.**

I. Introduction

The scalability limit of traditional sector-based Air Traffic Control (ATC) services, i.e., difficulty in subdividing heavily loaded sectors, is becoming a barrier to the sustainable growth of air traffic. Researchers have started examining and testing the concept of flow-centric operation [1], which views the whole regional airspace and controls groups of flights throughout their flight segments in a region. It opens the opportunity to distribute air traffic more efficiently in the airspace without being constrained by sector boundaries.

One primary challenge in flow-centric operation is the efficient coordination of air traffic flow at the intersections to avoid inefficiencies that may jeopardize flight safety [2]. Research focusing on sector-based air traffic coordination, such as sector traffic prediction and flow optimization for workload balancing between sectors [3], no longer adapts flow-centric operations where coordination is primarily used to avoid potential inefficiencies or conflicts between the intersecting air traffic flows. Therefore, it is crucial to develop a flow-centric framework that can identify, predict, and dynamically coordinate the evolving air traffic flows. For instance, traffic flow can be strategically re-routed when the predicted demand exceeds the acceptable flow limit at flow intersections.

Effective air traffic flow identification is the cornerstone for flow-centric air traffic analysis, prediction, and coordination [2]. In the literature, air traffic flow has been described according to airspace configuration, such as the groups of flights transiting through area control centers, waypoints, sectors, and airways [4]. Such a characterization of air traffic flow fits the traditional Air Traffic Control (ATC) paradigm where ATC units are geographical sectors and flights follow airways consisting of fixed waypoints. However, flow-centric operations require identifying the evolving air traffic flow patterns, such as flow locations and structures, disregarding the fixed airways and sectors. Fig. 1 shows one-day flight trajectories (pink lines) in French airspace, where nearly 50% above 19500ft is free route airspace (a potential coupled working method to flow-centric operations). It can be observed that the positions of airports and scheduled flights between airports restrict air traffic to an appropriate pattern of main flows [5]. Thus, identifying Nominal Flow Intersections (NFI) by constructing and analyzing air traffic flow patterns is the first enabler of effective flow coordination.

In addition to NFI identification, effective flow coordination requires constantly viewing air traffic demand according to the available capacity at the NFIs. In the literature, aggregated air traffic flow prediction mainly predicts the number of flights transiting through different airspace locations, such as entry-exits, origin-destinations, and air routes [6]. The time series of traffic demand at single or multiple airspace locations are used as the input to predict the future demand using Long Short-Term Memory (LSTM) [7], Convolutional Neural Networks (CNNs) [8], and Graph Convolutional Networks (GCNs) [4]. While time series flow features provide prediction models with information on the number of flights, the most important characteristic of air traffic flow, the "flow of flights in the airspace," can not be depicted by a time series, limiting the prediction accuracy [9]. Moreover, most flow prediction models adopt recurrent neural networks, in which data are processed one after another to learn the sequential relations in a time series, making it difficult to track long-term relations

SESAR Innovation Days
27-30 November 2023
Seville

in the input sequence [10]. Therefore, developing an effective flow feature representation to describe the dynamics inside air traffic flow and a prediction model that can learn relevant features between sequential elements far from each other is the second enabler of flow coordination.

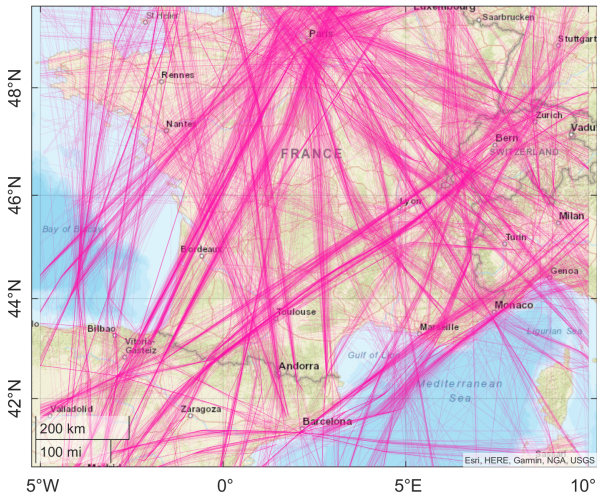

Figure 1: One-day flight trajectories in French airspace: flight trajectories are aggregated as flows connecting major hubs.

Besides air traffic prediction at the NFIs, it is essential to know the acceptable flow limit at the NFIs, given the NFIs can be overloaded due to excessive air traffic flows. In traditional sector-based ATC systems, the sector capacity is usually quantified as the maximum hourly number of flights that may enter a sector over a sustainable period while maintaining a safe, orderly, and efficient traffic flow [11]. Similarly, in flow-centric ATC systems, if the demand at an NFI exceeds the acceptable limit, the efficiencies and safety of air traffic flow at the NFI can be compromised. Airspace capacity estimation methods in the literature, such as the Monitor Alert Parameter (MAP) model [12], the full workload model (considering transit, recurring, conflict, and background workload) [11], the sector merge/split-based model [13] are primarily tailored to sector-based operations which cannot accommodate the flow-centric requirements. Therefore, a flow-centric algorithm for flow acceptance limit identification at the NFIs is the third enabler of effective flow coordination.

When the predicted air traffic demand exceeds the corresponding acceptable flow limit at an NFI, a flow coordination model will be required to re-configure the air traffic demand at the NFIs in advance to restrict the air traffic flow within a level not overloading the system excessively [14]. In traditional sectors, air traffic overload is managed by sector operations such as merging and splitting [15]. Under the flow-centric paradigm, traffic flow density and complexity change over time, rendering static flow control operations underloaded or overloaded. Dynamic flow re-configuration, such as flow merge/split/re-routing, gives flow-centric airspace an option to address the overload at NFIs without compromising the flow demand. Therefore, developing a dynamic flow re-configuration model subject to the time-varying traffic flows is the fourth enabler of efficient flow coordination decisions.

Given the above analysis, this paper proposes a dynamic air traffic flow coordination framework to identify, predict, and re-route air traffic flows to enable more efficient flow-centric airspace management. Firstly, a graph-based flow pattern consistency analysis approach is proposed to identify nominal air traffic flow intersections (NFIs) in the airspace through modeling and analyzing daily air traffic flow patterns. Secondly, a text-enriched flow feature representation is proposed to describe "the flow of flights" in the airspace using a "text paragraph" composed of the time and flight sequences at the NFIs. Compared to traditional time series representation describing "how many flights were in the airspace," it describes not only the number of flights but also the flow patterns shaping the movement of air traffic. A transformer-encoder-based neural network model is adopted to learn correlations among flow sequences to predict the future traffic demand at the NFIs. Thirdly, for each NFI, the acceptable flow limit is determined by identifying the phase transition of the flow efficiency, characterized by the flight transition duration from its neighboring NFIs versus the traffic demand during different periods. Finally, a reinforcement learning-based flow re-routing model is proposed to dynamically assign alternative routes to air traffic flows, especially when the predicted demand exceeds the acceptable limit, considering the effects of route assignment on flow efficiency and demand at NFIs during both current and future periods.

II. Methodology

A. Methodology Overview

The proposed air traffic flow coordination framework consists of four main steps: a) NFI identification through exploration of air traffic flow patterns; b) NFI flow feature representation and demand prediction during different periods; c) NFI flow acceptance limit determination through identifying phase transitions in flow transition duration; d) NFI flow re-routing agent design and training using reinforcement learning to avoid flow excess and improve flow efficiency.

Fig. 2 presents a concept diagram of the proposed framework. Firstly, the proposed method identifies NFIs through trajectory intersection clustering. The cluster centers are the NFIs. The number of clusters is determined by graph analysis of daily air traffic flow patterns, represented by a graph whose nodes are the NFIs, and edges describing flight connectivity between the nodes. The optimal number of NFIs is determined by evaluating the daily graph pattern consistency based on the node locations and edge structures.

Secondly, inspired by Natural Language Processing (NLP), the "flow of flights in the airspace" during a period is described by a text paragraph consisting of the sequences of flights transiting through the NFIs. In NLP, a sentence consists of a sequence of words governed by grammar and is used by neural networks to extract linguistic features for downstream tasks such as next-word prediction and sentiment analysis [16]. Meanwhile, the "flow of flights in the airspace" during a period consists of sequences of flights at different locations governed by recurrent traffic flow patterns. Analogously,

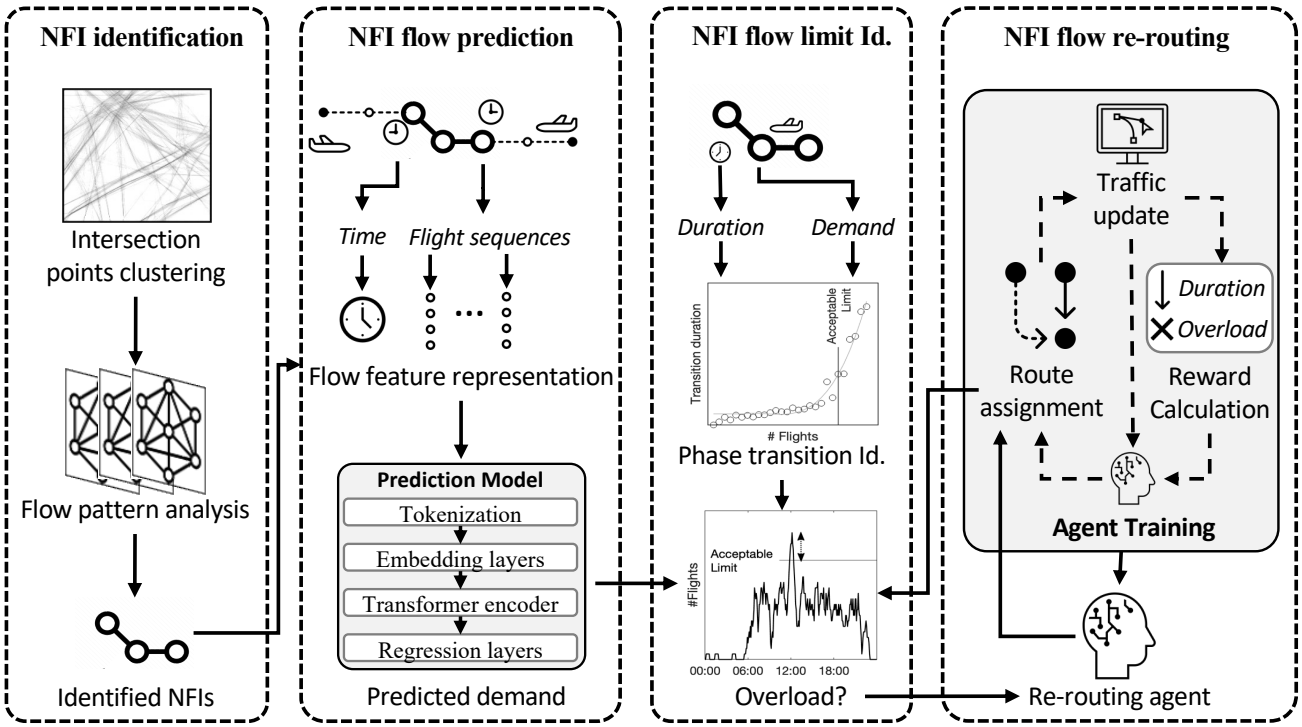

Figure 2: Conceptual diagram of the proposed machine-learned traffic flow coordination Framework. The NFIs are identified through graph pattern analysis. Then, flow features are represented as the time and flight sequences at NFIs, used by the transformer encoder-based model to predict future demand. Comparing the prediction and the flow limit can identify the overload at NFIs. Overload can be avoided by alternative route assignment from the flow re-routing agent.

learning from flow features represented by flight sequences at NFIs during different periods has the potential to achieve air traffic prediction tasks. Moreover, the transformer encoder architecture, using the attention mechanism to enable dynamic highlighting of relevant features between input elements and parallel sequence processing [17], is adopted to capture the relations among flows represented by the flight sequences to predict the flight demand at the NFIs during different periods.

Thirdly, when an NFI is overloaded, air traffic congestion can be induced, and it will take longer for air traffic transiting to the overloaded NFI due to regulatory measures such as vectoring and speed control [18]. Therefore, the flow acceptance limit at each NFI is identified as the demand above which the flow efficiency reduces significantly, i.e., the flight transition duration from neighboring NFIs to the NFI increases distinctly.

Finally, to improve flow efficiency while preventing adverse effects of flow re-routing during the current period over future air traffic, this paper considers flow re-routing as a sequential decision-making problem [19] where the action of alternative route assignment to a flow has consequences affecting future flow efficiency and flow demand at the NFIs. Then, deep reinforcement learning algorithms are adopted to train an agent to dynamically assign alternative routes to air traffic flows based on the evolving traffic flow states, considering the effects of route assignment on both current and future periods to reduce flight transition time in the airspace without exceeding the flow limit at the NFIs. The following sections illustrate the detailed procedures of the four steps.

B. NFI Identification

This paper identifies the NFIs through flight trajectory analysis using ADS-B data, including intersection points clustering, daily flow pattern representation, and graph analysis.

1) Intersection Points clustering: A trajectory intersection point is identified when two flights fly at adjacent flight levels, and their trajectories intersect when mapped onto the earth's surface. The time difference between the two flights passing the intersection is within 30 minutes, a widely used time window in the literature on air traffic flow management, flight planning, and capacity estimation [20].

With the trajectory intersections computed from flight track data, clustering algorithms are adopted to organize the intersection points into representative NFIs. Hierarchical clustering decomposes the data based on group similarities to find a multilevel hierarchy of clusters [21]. Considering the hierarchical organization of air traffic flows connecting regional feeders to international hubs [22], [23], this paper adopts single-linkage hierarchical clustering of trajectory intersections to discover the natural organization of flow intersections:

$$\begin{aligned} obj = \quad & \arg\max_{V(n)} \sum_{r=1}^{n-1} \sum_{s=r+1}^{n} \sum D(r,s) \\ s.t. \quad & D(r,s) = min(dist(x_{ri}, x_{sj})) \end{aligned} \tag{1}$$

where x_{ri} and x_{sj} are the i and j-th object in cluster r and s. n is the number of clusters. $V(n)$ denotes the cluster centers.

2) Flow Pattern Analysis: If the number of clusters is too large, the clustering result will be susceptible to small fluctuations in air traffic flow. When the number of clusters is too small, the identified NFIs can largely deviate from actual flow paths. The consistent and dependable performance of airspace users is an essential requirement for improving ATM system predictability [24]. The identified NFIs should represent the consistency of air traffic flow patterns while

considering daily flow alternations. Thus, the geographical and structural consistencies of air traffic flows versus the number of clusters are analyzed to determine the optimal number. The flow pattern consistency is evaluated from two perspectives: a) geographical consistency in NFI locations and b) structural consistency in flow connectivity between NFIs.

The daily air traffic flow pattern is represented by a weighted graph $G = (V, E)$ [25], where V is the set of nodes denoting the NFIs. The flow connectivity between nodes is described by the weighted edges E. The edge weight is quantified by the air traffic volume on the edge.

a) Geographical Consistency in NFI locations: A nearest-neighbor-based analysis is conducted to measure the geographical consistency of the daily NFI locations. Given a number of n nodes in the graph G_k constructed for the k-th day, let $V_k = \{v_{k,1}, v_{k,2}, ..., v_{k,i}, ..., v_{k,n}\}$ represent the set of nodes. Similarly, let $V_{k+1} = \{v_{k+1,1}, v_{k+1,2}, ..., v_{k+1,j}, ..., v_{k+1,n}\}$ represent the set of nodes in the graph G_{k+1} for day $k+1$. For each node $v_{k,i}$ in V_k, the proposed algorithm searches for its nearest node v_{k+1,a_i} in V_{k+1} according to the great circle distance [26]. a_i is the index of the identified nearest node of $v_{k,i}$ in V_{k+1}.

Through the above calculations, the nearest neighbouring node v_{k+1,a_i} of node $v_{k,i}$ for $i = 1, ..., n$ can be determined. Similarly, the nearest neighbouring node v_{k,b_j} of node $v_{k+1,j}$ for $j = 1, ..., n$ can be determined. b_j is the index of the identified nearest node of $v_{k+1,j}$ in V_k. Therefore, two sets of matched node pairs can be obtained: $MP_k : (v_{k,1}, v_{k+1,a_1}), (v_{k,2}, v_{k+1,a_2}), ..., (v_{k,n}, v_{k+1,a_n})$ and $MP_{k+1} : (v_{k,b_1}, v_{k+1,1}), (v_{k,b_2}, v_{k+1,2}), ..., (v_{k,b_n}, v_{k+1,n})$. Then, the geographical consistency of node locations is quantified as the number of mutually matched nodes divided by the total number of nodes, which is formulated as:

$$gc_1 = \frac{|MP_k \cup MP_{k+1}|}{n} \tag{2}$$

$|MP_k \cup MP_{k+1}|$ represents the number of node pairs in the union of MP_k and MP_{k+1}, denoted as l in the paper.

b) Structural Consistency in Flow Connectivity: Upon determining the geographical consistency in NFI locations, the next step is quantifying the structural consistency in the daily air traffic flow connectivity between the NFIs. Let $Sub = MP_k \cup MP_{k+1}$ represent the set of mutually paired nodes from graph G_k and graph G_{k+1}. $C_k = \{c_{k,1}, c_{k,2}, ..., c_{k,l}\}$ denotes the nodes in Sub from graph G_k, and $C_{k+1} = \{c_{k+1,1}, c_{k+1,2}, ..., c_{k+1,l}\}$ denotes the corresponding paired nodes from G_{k+1}. Let W_{c_k} and W_k represent the weighted adjacency matrix of C_k and V_k. The entry $w^{i,j}_{c\_k}$ represents the weight on the edge connecting nodes $c_{k,i}$ and $c_{k,j}$. The entry $w^{i,j}_k$ represents the weight on the edge connecting nodes $v_{k,i}$ and $v_{k,j}$. The structural consistency of the air traffic flow patterns is measured by the mutual flow connectivity in the two graphs. More specifically, it is evaluated by the ratio of mutual flow connections between the graphs characterized by nodes C_k and C_{k+1} compared to the union of flow connections in G_k and G_{k+1}:

$$gc_2 = \frac{\sum_{i=1}^{l-1}\sum_{j=i+1}^{l} min(w^{i,j}_{c\_k}, w^{i,j}_{c\_k+1})}{\sum_{i=1}^{n-1}\sum_{j=i+1}^{n}(w^{i,j}_k + w^{i,j}_{k+1})} \tag{3}$$

The optimal cluster number $n = N_v$ is determined by graph pattern analysis to find the saddle point, i.e., local maxima, of the daily graph pattern consistency versus the cluster numbers:

$$\begin{aligned} P(n) = \quad & \arg\min_n \sum (P(n) - \tfrac{gc_1(V(n)) + gc_2(V(n))}{2}) \\ s.t. \quad & P'(n) = 0; P''(n) < 0 \end{aligned} \tag{4}$$

where $P(n)$ is the polynomial approximation of the average of gc_1 and gc_2 (scaled between 0 and 1). As shown in Fig. 3, the circle marks the identified saddle point N_v on $P(n)$.

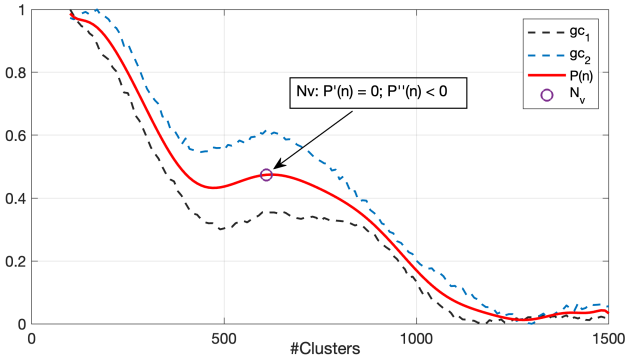

Figure 3: Determination of the cluster number through saddle point identification on $P(n)$, the polynomial approximation of the average of graph pattern consistency gc_1 and gc_2 (scaled between 0 and 1), versus the cluster number.

C. Flow Prediction at NFIs

1) Text-enriched Flow Description: With the N_v NFIs, the flow features at the k-th NFI is represented as a sequence $s_k = \{f_{k,1}, f_{k,2}, ..., f_{k,m_k}.\}$ of the m_k flights transited through the NFI during the past period t_p, e.g., past one hour. Each flight is denoted by its callsign text. If no flights are transiting through an NFI, the callsign sequence for this NFI will be described by the phrase: "No flights.". The flow feature in the airspace during t_p can be represented as the concatenation of flight sequences at different NFIs during t_p:

$$S = Concat(t_p, s_1, s_2, ..., s_{N_v}) \tag{5}$$

2) Transformer Encoder-based Flow Prediction Model: The flow features for various periods are the inputs to the transformer-encoder-based model to learn the flow relations in the sequence and predict the future air traffic flow. Let $\mathcal{S}$ be the space of all possible input text sequences S and $\mathcal{Y}$ be the space of all possible future traffic demand sequences Y during the future N_p periods. The flow prediction model $f(\cdot)$ learns the mapping: $\mathcal{S} \overset{f(\cdot)}{\rightarrow} \mathcal{Y}$. Fig. 4 shows the neural network structure for flow prediction at NFIs, consisting of tokenization, embedding, transformer encoder blocks, and a fully connected layer.

a) Tokenization: Given an input sequence, including the time and the flight sequences at the NFIs, word tokenization [27] is applied to convert elements in the input sequence S into

a list of integers $X = x_1, x_2, ..., x_m\}$ that can be embedded into a vector space.

b) Embedding: The token embedding layer converts the tokenized flow sequence into a list of vectors. Given a token x_i, its embedding $TE(x_i) \in \mathbb{R}^{d_{model}}$ can be represented as: $TE(x_i) = \mathbf{W}_e x_i$ where $\mathbf{W}_e$ is the embedding matrix and d_{model} is the embedding dimension. Positional embedding $PE(x_i)$, generated using trigonometric functions (sines and cosines) to provide a sinusoidal pattern encoding the position information, are added to the token embeddings as the input to the transformer encoders.

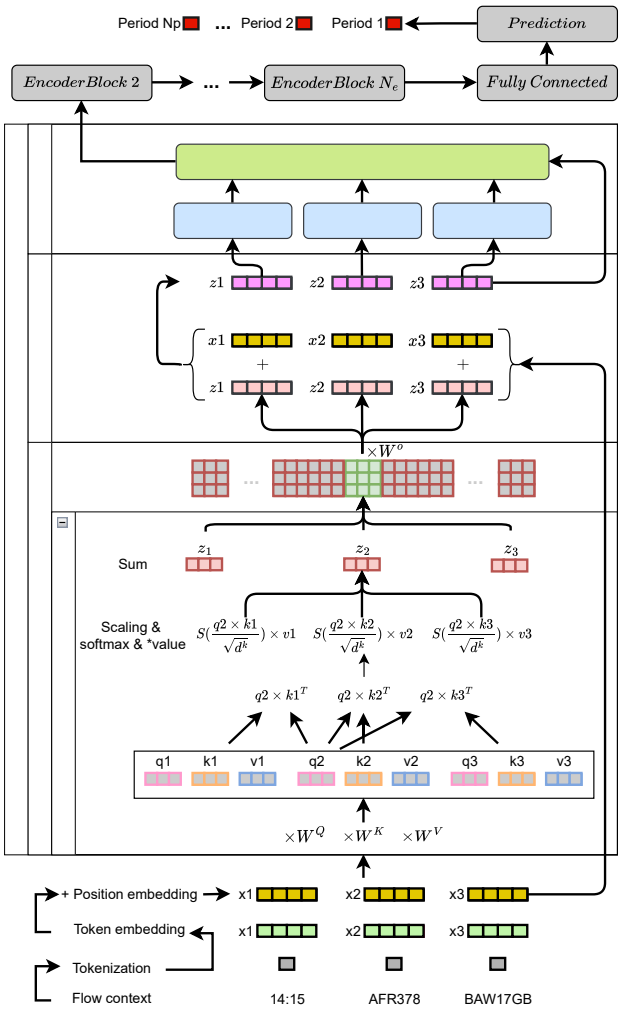

Figure 4: Proposed transformer-based framework for the flow prediction model. For instance, multiplying $x2$, the embedded vector for the callsign "AFR378", by W^Q, W^K, W^V produces the query, key, and value vectors $q2$, $k2$, and $v2$ associated with "AFR378". When processing the self-attention for "AFR378", its first attention weight related to element "14:15" would be $S(\frac{q2 \times k1}{\sqrt{d^k}})$. Multiplying each value vector by the attention weight and summing up the weighted value vectors produce the output of the self-attention layer.

c) Transformer Encoder Blocks: The output of the input sequence embedding $E(X)$ in which $E(x_i) = TE(x_i) + PE(x_i)$ is the input to the stack of N_e transformer encoder blocks to process each element in the input sequence and compile the information it captures into a context tensor.

Each encoder block has two major components: the multi-head self-attention mechanism and the position-wise fully connected feed-forward network [28]. The self-attention mechanism allows the encoder to look at other elements in the input sequence when encoding a specific element. It creates three vectors, query $Q = E(X)\mathbf{W}_Q$, key $K = E(X)\mathbf{W}_K$, and value $V = E(X)\mathbf{W}_V$, for each input element by multiplying the embedding with weight matrices W^Q, W^K, and W^V. The three vectors are used to score the relevance of other elements in the sequence against the specific element calculated by: $Softmax(\frac{QK^T}{\sqrt{d_{head}}})V$. d_{head} denotes the dimension of the head, e.g., the dimension d^k of the key. Multi-headed attention runs through a self-attention mechanism several times in parallel, which allows the model to jointly attend to information from different representation subspaces at different positions [17]. The output of the multi-head attention is added element-wise to the original input embeddings and normalized using layer normalization. Its output, represented by $A\&N_1$, is then passed through the feedforward network $FFN(A\&N_1)$ of the encoder block. The final output of the encoder block is:

$$A\&N_2 = LayerNorm(FFN(A\&N_1) + A\&N_1) \quad (6)$$

The output from the stack of N_e encoders is forwarded to a fully connected layer $Y = FFN(A\&N_2(N_e))$ to obtain the flow prediction results for different prediction windows, i.e., future period 1, period 2,..., and period N_p.

D. NFI Flow Acceptance Limit Identification

When the demand at an NFI is above the acceptable limit during a period, air traffic congestion can happen, and it will take a significantly larger time cost for air traffic transiting to the overloaded NFI on their flight paths due to regulatory measures such as vectoring and speed control.

During period t, flight transition durations from NFI v_j to NFI v_i are denoted as $H_{ij,t}$. $H_{ij,t}$ is normalized by the daily minimum duration $h_{ij,t}$ regarding t to reduce the effects of daily fluctuations in air traffic flow:

$$NH_{ij,t} = \frac{H_{ij,t}}{h_{ij,t}} \quad (7)$$

Let $NH_{i,t} = \{NH_{ij,t}\}$ denote the normalized transition duration to v_i of all NFIs connected to v_i during period t. Let $NH_i = \{NH_{i,t}\}$ denote the flight transition duration to v_i for all periods $t \in \{1, 2, ..., N_T\}$ in the traffic data. Let $n_i = \{n_{i,t}\}$ denote the corresponding traffic demand during $t \in \{1, 2, ..., N_T\}$. $n_{i,t}$ is the total number of flights transiting to v_i during t. By fitting the demand values to the transition duration values, a set of demand values $\{1, 2, ..., n\}$ and the corresponding transition duration value $\{y_1, y_2, ..., y_n\}$ can be obtained. The flow acceptance limit at v_i is determined by identifying the demand l_i above which the transition duration of flights to v_i will increase abruptly, which is formulated as:

$$\begin{aligned} obj = \quad & \arg\min_{l_i} \quad (l_i)var([y_1, ..., y_{l_i}]) \\ & +(n - l_i)var([y_{l_i+1}, ..., y_n]) \end{aligned} \quad (8)$$

If there is no abrupt change detected, indicating no explicit trend concerning the flow demand based on the observations, the flow limit at the NFI is determined as the maximum flow demand observed.

E. Reinforcement Learning based Flow Coordination

This section adopts reinforcement learning algorithms to train an agent for flow re-routing to avoid flow excess and improve flow efficiency. During the t-th period, the agent assigns a route for a main flow according to the re-routing policy $\pi_\theta\left(a_t|s_t\right)$ parameterized by θ. $\pi_\theta\left(a_t|s_t\right)$ determines the agent's action $a_t \in A$, i.e., which route to take, regarding the traffic state $s_t \in S$. S represents the state space of the traffic flow described by the traffic volumes at the NFIs. A represents the action space, consisting of the alternative routes a flow can take. $R\left(s_t, a_t\right)$ denotes the agent's reward of taking action a_t in s_t based on whether the flow excess is avoided and how much the flow efficiency is improved:

$$R\left(s_t, a_t\right) = e_t\left(T_t^{(0)} - T_t^{(s_t,a_t)}\right)/N_{flights} \tag{9}$$

where $e_t = 1$ otherwise 0 if the flow excess is avoided and no new excess at other NFIs is induced. $T_t^{(0)}$ is original flight exit time in the airspace during the t-th period, while $T_t^{(s_t,a_t)}$ represents the time by taking an alternative route a_t. $N_{flights}$ denotes the number of flights transited through the re-routing area during the t-th period.

The agent's objective is maximizing the expected cumulative reward over time, represented by the objective function:

$$J(\theta) = \mathbb{E}\left[\sum_{t=0}^{T}\gamma^t R(s_t, a_t)\right] \tag{10}$$

where T is the learning horizon. γ is the discounting factor.

This paper adopts the Proximal Policy Optimization (PPO) [29] to train the agent, which introduces a surrogate objective with a clipping mechanism preventing significant policy updates to improve sample efficiency and stability:

$$\begin{aligned} arg \quad & \max_{\theta} \mathbb{E}\left[min(\tfrac{\pi_\theta(a_t|s_t)}{\pi_{\theta_o}(a_t|s_t)}A^{\pi_{\theta_o}}\left(s_t,a_t\right), g\left(A^{\pi_{\theta_o}}\left(s_t,a_t\right)\right))\right] \\ s.t. \quad & A^{\pi}\left(s_t,a_t\right) = \delta_t + (\gamma\lambda)\delta_{t+1} + ... + (\gamma\lambda)^{T-(t+1)}\delta_{T-1} \\ & g\left(A\right) = \begin{cases} (1+\epsilon)\,A, & A \geq 0 \\ (1-\epsilon)\,A, & A \leq 0 \end{cases} \\ & \delta_t = R\left(s_t,a_t\right) + \gamma V^{\pi}(s_{t+1}) - V^{\pi}(s_t) \end{aligned} \tag{11}$$

where $\pi_{\theta_o}\left(a_t|s_t\right)$ is the old policy from the previous iteration. $A^{\pi}\left(s_t,a_t\right)$ is the Generalized Advantage Estimation (GAE) estimating the advantage of taking action a_t compared with the average action in state s_t. $V^{\pi}(s_t)$ is the state value function of the expected cumulative reward starting from s_t. ϵ and λ are hyperparameters controlling the extent of clipping and the balance between bias and variance of GAE, respectively.

III. Experimental Study

To verify the efficacy of the proposed flow coordination framework, an experimental study has been carried out on the French airspace using one-month ADS-B data from 1 to 31 December 2019, comprising 158,856 flights. This study focuses on the en-route air traffic above 10,000 ft.

A. NFI Identification

This paper calculated the geographical consistency gc_1 and the structural consistency gc_2 against different cluster numbers ranging from 100 to 1500. A "saddle point" is observed for gc_1 and gc_2 at cluster number 605. Therefore, this paper takes 605 as the number of clusters. The cluster centers are determined as the NFIs. The 605 identified NFIs are denoted by "NFI1" to "NFI605" in this paper.

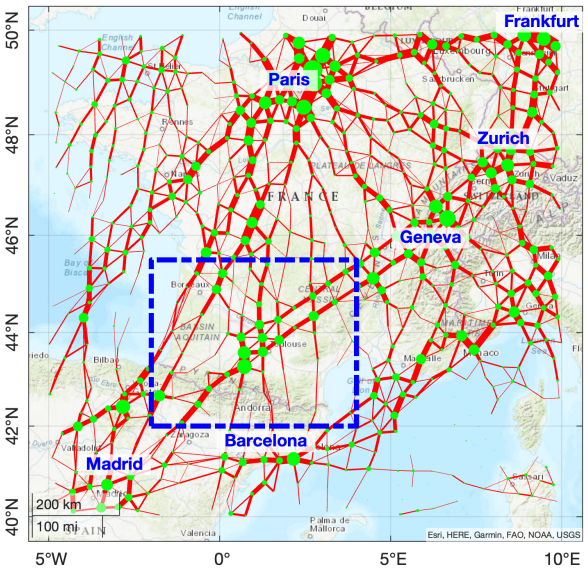

Figure 5: Graph representation for the one-month air traffic flow using 605 NFIs. The area confined by blue dashes is used for testing the flow re-routing model.

Fig. 5 shows the graph representation for the one-month air traffic flow with 605 NFIs. This graph can depict the nodal hierarchy of air traffic flows ranging from regional feeders to international hubs, such as Paris and Geneva. The en-route air traffic flows are organized as a series of "spokes" connecting the traffic hubs or connecting outlying areas to a hub area.

B. NFI Flow Prediction and Flow Limit Identification

The prediction model in this study adopts a stack of 12 transformer encoder blocks: $N_e = 12$. The model input is the flight callsign sequences on the identified NFIs during the past one hour. The model output is the number of flights transiting through the NFIs in the future 30 minutes. The Mean Square Error (MSE) between the prediction and the truth is used to compute the model's loss function. The number of trainable parameters is at the level of 10^8. The training batch size is 16. The learning rate is 0.00002. Air traffic data from 1st to 19th December 2019 are used for model training, the following six days of data for model testing, and the rest six days for model validation during training.

Table I shows the quantified prediction performance of the proposed method tested on three busy NFIs in the airspace, including NFI460 over the Paris area control center, NFI365 over the Geneva area control center, and NFI135 over the

TABLE I: PREDICTION PERFORMANCE ON THREE MAJOR NFIS OVER THE PARIS (NFI460), GENEVA (NFI365), AND BORDEAUX (NFI135) AREA CONTROL CENTERS IN TERMS OF MAE, MSE, MAPE, AND R^2.

NFI	MAE	MSE	MAPE	R^2
1: NFI460	2.339	12.184	0.217	0.951
2: NFI365	0.800	2.702	0.127	0.978
3: NFI135	0.984	2.929	0.145	0.977

border of Bordeaux and Madrid/Barcelona control centers. Four metrics are used for the performance evaluation: Mean Absolute Error (MAE), Mean Squared Error (MSE), Mean Absolute Percentage Error (MAPE), and R-squared (R^2). It can be observed that the prediction can accurately capture flow demand changes with MAE values smaller than one and MAPE values smaller than 0.15 for NFI365 and NFI135. The R^2 values of the prediction on the three NFIs are above 0.95, showing the predicted values can reliably approximate the true demand values. A more detailed illustration of the performance of the prediction model under different prediction windows and the comparison with other state-of-the-art methods can refer to the previous paper that specifically focuses on the flow prediction part of the framework [5].

Calculating the flight transition duration to the NFIs during different periods and under different traffic flow demands and observing the point of demand above which the flight transition durations increase sharply identifies the flow acceptance limit at NFIs. Fig. 6 shows flight transition duration versus the flow demand on four example NFIs. The blue circles show the original observations from the traffic data, the solid red lines show the fitted curves of the observations, and the pink dashes bound the 95% confidence intervals of the fitting. The curves of duration-demand are fitted using third-degree polynomials. The solid black line indicates the identified acceptance limit of the NFIs. Such phase transitions are observed on 68% of the NFIs, while the transition durations to the rest of the NFIs show no explicit trend concerning the flow demand based on the observations from the one-month data. The reason may be that traffic flow demand on these NFIs is below capacity during this month, so there are no observations for their overloaded circumstances. The flow acceptance limits on such NFIs are set as the maximum flow demand observed this month.

The blue lines in Fig. 7 show instances during six days in December 2019 where the traffic demand on NFI135 exceeded the acceptable limit. The horizontal axis shows the time, and the vertical axis shows the next 30-minute demand. NFI135 is a major NFI where cross-border flows between Bordeaux and Madrid/Barcelona air traffic control centers are transiting through. Flow demand exceeding the acceptable limit is commonly observed on NFI135. Thus, NFI135 is used to demonstrate the flow coordination result to examine the efficacy of the proposed models in re-routing the traffic flows to improve flow efficiency.

C. NFI Flow Excess Re-routing

As shown in Fig. 8, the flow originating from NFI 505 (green dot) and heading to NFI279 (blue dot) is the major flow

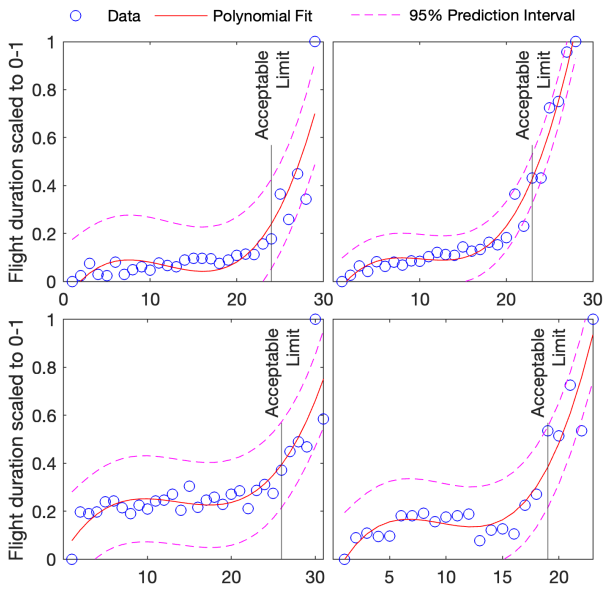

Figure 6: Flight transition duration (y-axis) versus the flow demand (x-axis) on four NFIs. The black vertical lines show the acceptable flow limit of the NFIs.

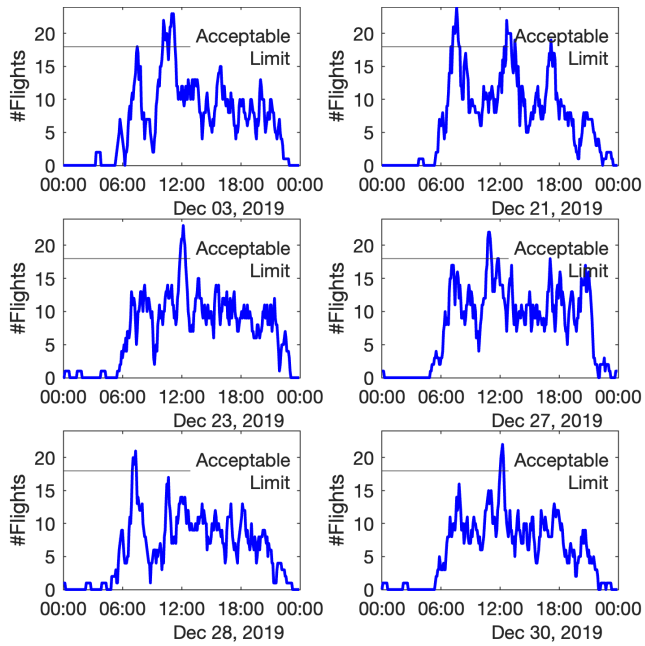

Figure 7: Instances of flow demand exceeding the acceptable limit are commonly observed on NFI135 during Dec 2019, where flow re-routing is to be applied to avoid the overload.

transiting through NFI135 (red dot). Fig. 8 also shows seven alternative routes that this flow may take, derived from the historical flight trajectories. The reinforcement learning-based re-routing agent is trained in the environment of the Bluesky ATC simulator [30]. Given the limited computational resources, the part of French airspace confined by $[42N, 45.5N, 2W, 4E]$, shown by blue dashes in Fig. 5, is chosen as the re-routing area inside which the agent's actions is generated and rewarded. The original flight trajectory is used as the planned flight path. Every 30 minutes, based on the traffic flow state, i.e., traffic demand at the NFIs during the past 30 minutes, the agent

dynamically selects one from the seven alternative routes for the flow "NFI505→NFI135→NFI279" to avoid flow excess at NFIs and reduce the flight transition time in the airspace.

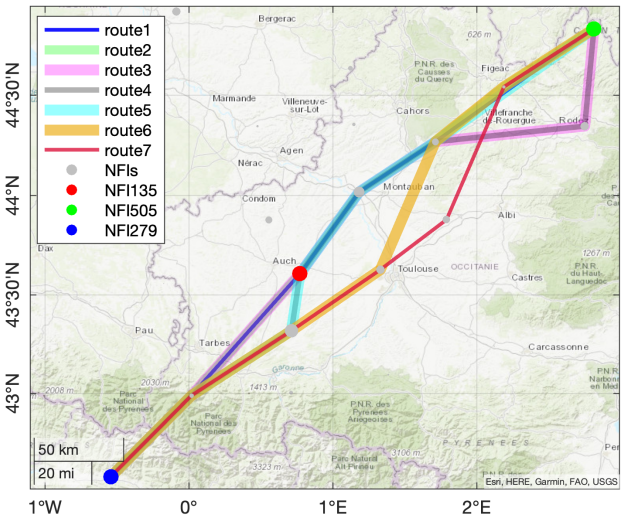

Figure 8: Alternative routes for air traffic flow transiting through NFI135.

The model is trained with the traffic scenarios during Dec 2019 when the demands exceeded the flow limit at NFI135. To consider the accumulated effects of the agent's re-routing decisions, the length of each training episode is set as 2 hours, which can also cover the travel time of most flights in the focal airspace. As shown in Fig. 9, the model converges to an optimal route assignment policy as the number of training steps increases. The mean reward of each episode fluctuates and continues to increase at the beginning and stabilizes at the value of 322.168 as the training step increases. It shows that, on average, the travel time of each flight in the re-routing area is reduced by 322.168 seconds during the 2-hour re-routing episode compared with the originally planned flows. Moreover, the explained variance of the value function increases towards one during training, showing the learned value function accurately models the environment's dynamics, and the predictions accurately match the true returns.

Fig. 10 shows the flow re-routing results from 1150UTC to 1250UTC on 24 Dec 2019 and 0700UTC to 0800UTC on 21 Dec 2019, where the demand exceeds the acceptable limit. For the period 1150UTC–1220UTC and 1220–1250UTC, the assigned flow route is "route 7" and "route 1" in Fig. 8 respectively, while for the period 0700UTC–0730UTC and 0730UTC–0800UTC, the assigned route is "route 6" and "route 7" in Fig. 8 respectively. Table II compares the traffic flow excess and efficiency before and after re-routing. It can be observed that the flow excess at NFI135 is avoided as the traffic flow demands every 30 minutes are below the acceptable limit after re-routing. For the 43 flights exiting the re-routing area during 1150UTC–1220UTC, there is a 9.58-minute reduction in flight time, and for the 51 flights exiting the re-routing area during 1220UTC–1250UTC, the reduction in flight time is 184.87 minutes. During 1150UTC–1250UTC, there is a total flight time reduction of 194.45 minutes for the 94 flights in the re-routing area. During 0700UTC–0800UTC,

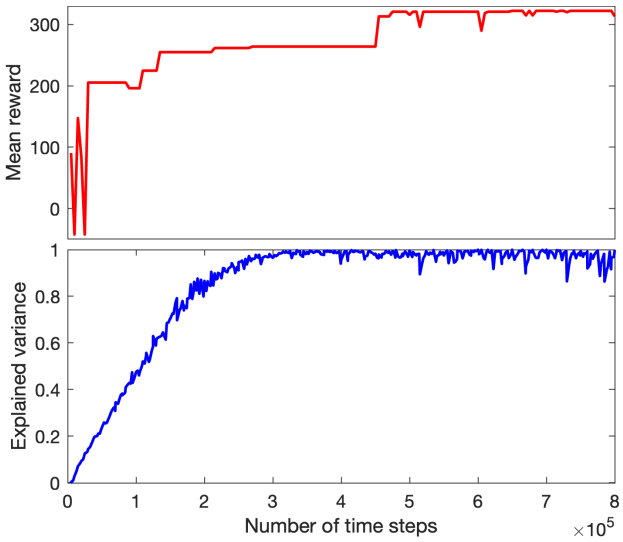

Figure 9: The re-routing model converges to the optimal policy during training.

there is a total flight time reduction of 266.33 minutes for the 100 flights in the re-routing area. After re-routing, air traffic in the airspace speeds up, and flight transition time is reduced compared to original flight routes.

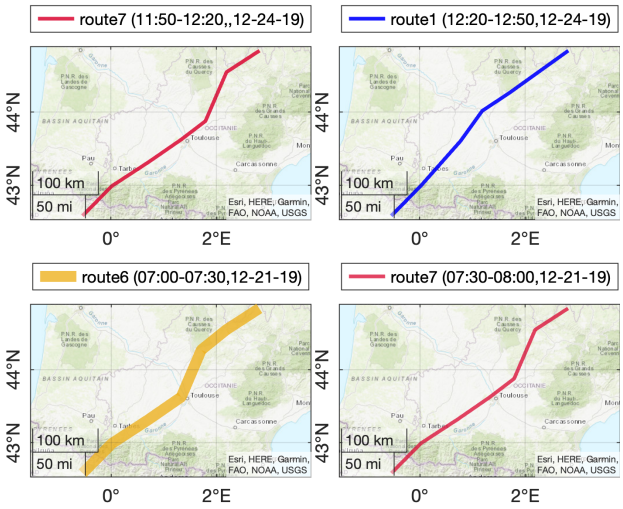

Figure 10: Re-routing results for air traffic flow transiting through NFI135.

It is noteworthy that the flight time reduction during the later periods (1220UTC to 1250UTC and 0730UTC to 0800UTC) significantly exceeds that observed during the earlier periods (1150UTC to 1220UTC and 0700 UTC to 0730UTC). This difference can be attributed to the cumulative effects of flow re-routing implemented in both the early and later periods, influencing air traffic throughout the later periods. Conversely, their effects on air traffic may not manifest fully during the earlier periods.

IV. Conclusions

Aiming to contribute to the future flow-centric paradigm, this paper proposes a flow-centric air traffic flow coordination framework to avoid overload at major flow intersections and improve efficiency. First, Nominal Flow Intersections (NFIs)

TABLE II: COMPARISON OF FLIGHT TRAVEL TIME REDUCTION OF TRAFFIC FLOWS BEFORE & AFTER RE-ROUTING.

time (UTC)	before		after		RTE	time reduction
	flow	XS.	flow	XS.		mins/flights
11:50-12:20 (24th)	18	0	9	0	7	9.583/43
12:00-12:30 (24th)	21	3	13	0	\	133.083/51
12:10-12:40 (24th)	23	5	13	0	\	174.200/51
12:20-12:50 (24th)	20	2	12	0	1	184.867/51
7:00-7:30 (21st)	18	0	13	0	6	16.167/32
7:10-7:40 (21st)	21	3	11	0	\	51.683/54
7:20-7:50 (21st)	20	2	11	0	\	150.583/59
7:30-8:00 (21st)	24	6	10	0	7	250.167/68

were identified through modeling and analyzing the consistency of daily air traffic flow patterns. Then, a text-enriched description of the flow and movement of flights at the NFIs was used by a transformer encoder-based neural network to learn the flow relations to predict future demands at the NFIs. The acceptable flow limits at NFIs were determined as the demand above which the flow efficiency, characterized by flight duration between NFIs, changed significantly. Finally, a reinforcement learning-based flow re-routing model was trained to assign alternative routes to air traffic dynamically to improve flow efficiency and avoid the foreseen overload. The re-routing agent is tested on the NFI135 handling cross-border flows between Bordeaux and Madrid/Barcelona air traffic control centers, using ADS-B data in Dec 2019. After re-routing, air traffic in the airspace speeds up, and flight time is reduced compared with using original flight routes. By integrating accurate flow prediction and dynamic re-routing capabilities into airspace management systems, flow-centric airspace can proactively optimize traffic flow, reduce delays, and enhance safety. This research and findings may contribute to the development of concepts of operations for flow-centric airspace.

ACKNOWLEDGMENT

This research is supported by the National Research Foundation, Singapore, and the Civil Aviation Authority of Singapore, under the Aviation Transformation Programme. Any opinions, findings and conclusions or recommendations expressed in this material are those of the author(s) and do not reflect the views of National Research Foundation, Singapore and the Civil Aviation Authority of Singapore.

REFERENCES

[1] C. Ma *et al.*, "Dynamic air traffic flow coordination for flow-centric airspace management," in *15th USA/Europe ATM Seminar 2023, Savannah, Georgia, USA*, 5-9 June, 2023.
[2] I. Gerdes *et al.*, "From free-route air traffic to an adapted dynamic main-flow system," *Transportation Research Part C: Emerging Technologies*, vol. 115, p. 102633, 2020.
[3] D. Chen *et al.*, "A network based dynamic air traffic flow model for en route airspace system traffic flow optimization," *Transportation Research Part E: Logistics and Transportation Review*, vol. 106, pp. 1–19, 2017.
[4] C. Ma *et al.*, "Sector entry flow prediction based on graph convolutional networks," in *ICRAT, Tampa, Florida, USA*, 19-23 June, 2022.
[5] M. Chunyao *et al.*, "Air traffic flow representation and prediction using transformer in flow-centric airspace," in *SESAR Innovation Days*, 5-8 December, 2022.
[6] Y. Zhang *et al.*, "A hierarchical heuristic approach for solving air traffic scheduling and routing problem with a novel air traffic model," *IEEE Transactions on Intelligent Transportation Systems*, vol. 20, no. 9, pp. 3421–3434, 2018.
[7] G. Gui *et al.*, "Machine learning aided air traffic flow analysis based on aviation big data," *IEEE Transactions on Vehicular Technology*, vol. 69, no. 5, pp. 4817–4826, 2020.
[8] Y. Lin *et al.*, "Deep learning based short-term air traffic flow prediction considering temporal–spatial correlation," *Aerospace Science and Technology*, vol. 93, p. 105113, 2019.
[9] K. Cai *et al.*, "Temporal attention aware dual-graph convolution network for air traffic flow prediction," *Journal of Air Transport Management*, vol. 106, p. 102301, 2023.
[10] R. T. Mutanga *et al.*, "Hate speech detection in twitter using transformer methods," *International Journal of Advanced Computer Science and Applications*, vol. 11, no. 9, 2020.
[11] J. Welch, "En route sector capacity model final report," *ATC-426*, 2015.
[12] B. Marr and K. Lindsay, "Controller workload-based calculation of monitor alert parameters for en route sectors," in *15th AIAA ATIO, Dallas, TX*, 22-26 June, 2015, pp. 3178–3188.
[13] D. Gianazza, "Learning air traffic controller workload from past sector operations," in *12th USA/Europe Air Traffic Management R&D Seminar, Seattle, United States*, 26-30 June, 2017.
[14] Y. Lin *et al.*, "From aircraft tracking data to network delay model: A data-driven approach considering en-route congestion," *Transportation Research Part C: Emerging Technologies*, vol. 131, p. 103329, 2021.
[15] Z. Liu *et al.*, "A framework for strategic online en-route operations: Integrating traffic flow and strategic conflict managements," *Transportation Research Part C: Emerging Technologies*, vol. 147, p. 103996, 2023.
[16] Y.-C. Zhou *et al.*, "Integrating nlp and context-free grammar for complex rule interpretation towards automated compliance checking," *Computers in Industry*, vol. 142, p. 103746, 2022.
[17] A. Vaswani *et al.*, "Attention is all you need," *Advances in neural information processing systems*, vol. 30, 2017.
[18] P. Baumgarten *et al.*, "The impact of hubbing concentration on flight delays within airline networks: An empirical analysis of the us domestic market," *Transportation Research Part E: Logistics and Transportation Review*, vol. 66, pp. 103–114, 2014.
[19] V. Singh *et al.*, "How are reinforcement learning and deep learning algorithms used for big data based decision making in financial industries–a review and research agenda," *International Journal of Information Management Data Insights*, vol. 2, no. 2, p. 100094, 2022.
[20] H. Balakrishnan and B. G. Chandran, "Optimal large-scale air traffic flow management," *Massachusetts Institute of Technology, Tech. Rep.*, 2014.
[21] Q. Cai and J. Liu, "Hierarchical clustering of bipartite networks based on multiobjective optimization," *IEEE Transactions on Network Science and Engineering*, vol. 7, no. 1, pp. 421–434, 2018.
[22] F. Seabra *et al.*, "Determinants of brazilian international flights: The role of hub-and-spoke and infrastructure variables," *Journal of Air Transport Management*, vol. 89, p. 101866, 2020.
[23] N. Adler *et al.*, "The multi-airline p-hub median problem applied to the african aviation market," *Transportation Research Part A: Policy and Practice*, vol. 107, pp. 187–202, 2018.
[24] M. C. R. Murça *et al.*, "Flight trajectory data analytics for characterization of air traffic flows: A comparative analysis of terminal area operations between new york, hong kong and sao paulo," *Transportation Research Part C: Emerging Technologies*, vol. 97, pp. 324–347, 2018.
[25] C. Ma *et al.*, "Airway network management using braess's paradox," *Transportation Research Part C: Emerging Technologies*, vol. 105, pp. 565–579, 2019.
[26] D. A. Prasetya *et al.*, "Resolving the shortest path problem using the haversine algorithm," *Journal of critical reviews*, vol. 7, no. 1, 2020.
[27] L. Sun *et al.*, "Spectral–spatial feature tokenization transformer for hyperspectral image classification," *IEEE Transactions on Geoscience and Remote Sensing*, vol. 60, pp. 1–14, 2022.
[28] Y. Zhao *et al.*, "Speech transformer with speaker aware persistent memory." in *INTERSPEECH*, 2020, pp. 1261–1265.
[29] J. Schulman *et al.*, "Proximal policy optimization algorithms," *arXiv preprint arXiv:1707.06347*, 2017.
[30] J. M. Hoekstra and J. Ellerbroek, "Bluesky atc simulator project: an open data and open source approach," in *ICRAT, PA, USA*, vol. 131. FAA/Eurocontrol USA/Europe, June 20-24, 2016, p. 132.